Aminopropyl functionalization of superparamagnetic iron oxide/SiO$_2$ nanocrystals for adsorption of bisphenol A from water

A. Farmany[a,*], M.M. Shirmohammadi[b], S. Kazemi[c], M. Hatami[d], S.S. Mortazavi[a]

[a]Department of Chemistry, Hamedan Branch, Islamic Azad University, Hamedan, Iran, emails: a.farmany@usa.com (A. Farmany), smortazavi58@yahoo.com (S.S. Mortazavi)
[b]Department of Engineering, Hamedan Branch, Islamic Azad University, Hamedan, Iran, email: mmshirmohammadi@gmail.com
[c]Faculty of Engineering, Bu-Ali Sina University, Hamedan, Iran, email: sh.kazemi93@yahoo.com
[d]Department of Chemistry, Hamedan University of Technology, Hamedan, Iran, email: mhatami@hut.ac.ir

ABSTRACT

Iron oxide nanocrystals synthesized by a co-precipitation method were decorated with an aminopropyl functionalized silica layer and characterized by Fourier transform infrared spectroscopy, X-ray diffraction, and scanning electron microscopy. Surface area of nanocrystals was measured using the N$_2$ adsorption–desorption Brunauer-Emmet-Teller procedure. Large surface area (208.0 m^2/g) of nanocrystals confirmed their potential for adsorption of organic/inorganic material. So the nanocrystals were used for adsorption of Bisphenol A (BPA) from aqueous solutions. As a continuation, the influence of different parameters including adsorbent dosage, pH, temperature, and ionic strength on the removal efficiency of BPA was studied. The experimental data were fitted well with the pseudo-second-order kinetic model ($R^2 = 0.99$). The adsorption isotherm was described well by the Freundlich isotherm.

Keywords: Water; Bisphenol A; Superparamagnetic iron oxide nanocrystal/SiO$_2$–NH$_2$; Adsorption

1. Introduction

Bisphenol A (BPA) is one of the highest production volume chemicals used in plastics and epoxy resins. This material has broad applications in food industry and medicine [1]. Biomonitoring studies support widespread exposure to BPA [2,3]. However, the exposure role of BPA in development of cancers (breast and prostate), alteration of immune functions, reduction of human sperm counts, prevalence of obesity, and decreased fertility in fish and mammals has been reported [4–6].

Therefore, removing the leached BPA from wastewater can minimize its potential harmful impact on humans.

At this time, numerous adsorbents such as minerals and carbon and carbon nanomaterials [7–9], soil column [10], lignin [11], hemimicells [12], highly ordered mesoporous carbon CMK-3 [13], and Metal-organic frameworks [14] have also been used for the removal of BPA. Iron oxide nanocrystals have shown prominent result for removal of contaminations from water [15–17]. These nanoparticles could become

*Corresponding author.

cost-effective nanomaterials for decontamination of chemical pollutions. Using iron oxide nanocrystals in adsorption process was believed to exhibit a high potential for the adsorption of organic/inorganic materials [18–20]. The advantages of superparamagnetic iron oxide nanocrystals such as efficient removal and easy separation motivated us to consider this nanomaterial as adsorbent for removal of BPA. In this study, the adsorption property of iron oxide nanocrystals for the removal of BPA from aqueous solution was investigated under different experimental conditions such as contact time, temperature, pH, and ionic strength. To evaluate the adsorption capacity further and understand the adsorption mechanism of iron oxide nanocrystal toward BPA, adsorption kinetics, and isotherms studies have also been estimated from the experimental results.

2. Experimental

2.1. Material and methods

All chemicals were of analytical grade and used as received. Ferrous chloride tetrahydrate ($FeCl_2 \cdot 4H_2O >$ 99%) ferric chloride hexahydrate ($FeCl_3 \cdot 6H_2O > 99\%$), sodium hydroxide (≥97%), and hydrochloric acid (37%), were purchased from Merck (Germany). (3-aminopropyl)-triethoxysilane (APTES, 99%) was purchased from Aldrich (Germany). All aqueous solutions were prepared with double distilled water. The Fourier transform infrared spectroscopy (FT-IR) spectra were recorded by an Infrared spectrophotometer coupled to (FT-IR, Perkin Elmer1600, USA).

2.2. Synthesis of superparamagnetic nanocrystal

Superparamagnetic iron oxide nanocrystals were prepared via an improved chemical co-precipitation method. Briefly, $FeCl_2 \cdot 4H_2O$ (1.5 mmol) and $FeCl_3 \cdot 6H_2O$ (3 mmol) prepared in 0.01 M hydrochloric acid was rapidly injected by a plastic tube to 80 mL 2 M ammonia solution. The system was stirred under N_2 for 1 h at room temperature. The precipitate was washed with pure ethanol and separated by magnetic decantation. Finally, superparamagnetic nanocrystals were dried under vacuum at 70°C.

2.3. Aminopropyl-triethoxysilane functionalizing superparamagnetic nanocrystal

A suspension of superparamagnetic nanocrystals was sonicated in 30 mL ethanol for 30 min to get uniform dispersion. A solution of 0.7 mL concentrated ammonia in 9.3 mL double distilled water was added to nanocrystal suspension. After 15 min of sonication, a solution of 1.8 mmol TEOS and 5 ml ethanol was injected to the sonicator. Sonochemical treatment was aged 2 h at room temperature. After 1 h of sonication, a very stable black colored magnetic fluid was obtained. The precipitate was collected with a magnet, and washed with ethanol (three times). Finally, functionalized superparamagnetic nanocrystal solid was obtained by ethanol evaporation at a reduced pressure chamber.

2.4. Batch adsorption method

Adsorption experiments were conducted using batch approach. Briefly, at room temperature, 50 mL solution contains 4 mg/L BFA and 0.2 mg naonocrystal added into a 50 mL flask. The pH of mixture fixed to 6. The suspension was mixed by a shaker for 35 min. The magnetic decanted supernatant was analyzed by UV–vis spectrophotometer. The removal sorption capacity of the sorbent was calculated by Eq. (1):

$$q_e = \frac{(C_0 - C_e)}{m} \times V \tag{1}$$

where q_e (mg/g) is the sorption capacity of the sorbent. C_0 (mg/L) is the initial BFA concentration, C_e (mg/L) is the equilibrium BFA concentration, m(g) is the sorbent mass, and V(L) is the volume of the solution.

3. Results and discussions

3.1. Superparamagnetic iron oxide/SiO₂–NH₂ characterization

3.1.1. FT-IR study

The FT-IR spectra of superparamagnetic iron oxide nanocrystal, and superparamagnetic iron oxide/SiO₂–NH₂ nancrystal are presented in Figs. 1 and 2. For both nanocrystals, absorption peaks at 581 cm⁻¹ were observed, which correspond to the Fe–O vibration of the magnetite phase of nanocrystal [21]. The binding of silica shell to iron oxide nanocrystal is apparent from FT-IR spectra (Figs. 1 and 2) where the following modes are observed: (a) vibration and stretching of SiO₂ at 1,221, 1,046, 991, and 993 cm⁻¹ which is in agreement with that reported by Huang et al. [19], (b) bending and stretching vibrations of amino functional groups at 2,808, 1,603, and 693 cm⁻¹ [18–21], and (c) stretching vibration of C=C groups of propyl functional groups at 2,800–3,025 cm⁻¹ [21]. In comparison between Figs. 1 and 2, significant changes in FT-IR spectra are observed when the aminopropyl functionalized iron
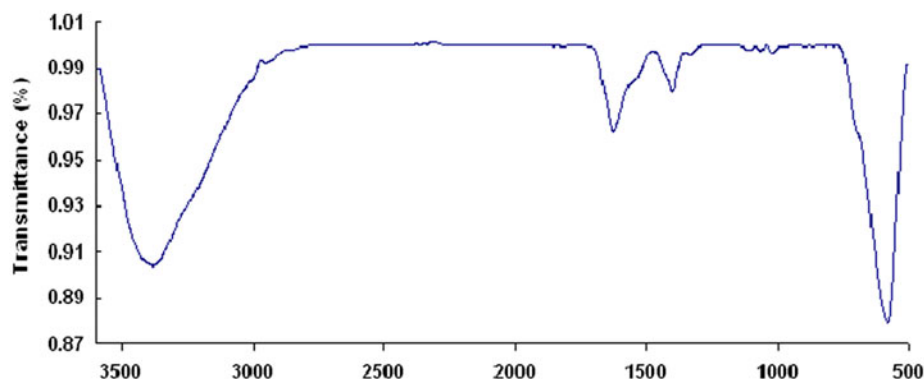
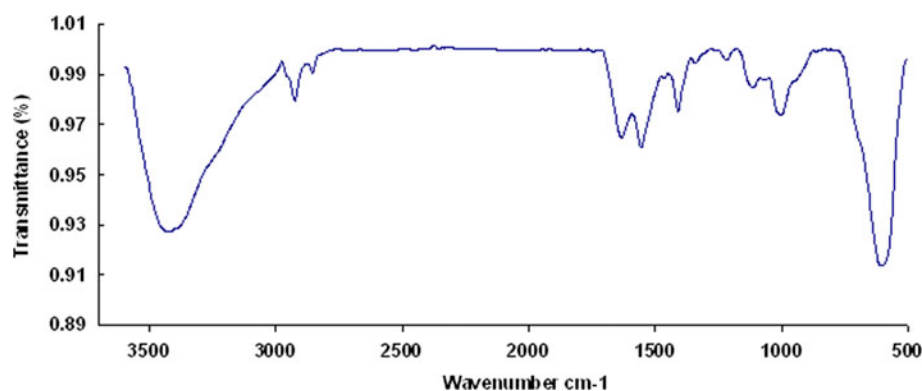Fig. 1. FT-IR of superparamagnetic Iron oxide nanocrystal.

Fig. 2. FT-IR of superparamagnetic Iron oxide nanocrystal/SiO_2–NH_2.

oxide nanocrystals are compared to the bare iron oxide nanocrystals. This indicates a strong binding of SiO_2 groups to the iron oxide nanocrystals and effective aminopropyl fictionalization process. Also, a comparison between FT-IR spectra of iron oxide nanocrystals and iron oxide/SiO_2–NH_2 in Figs. 1 and 2 indicates that iron oxide is coated by SiO_2 shell which Fe–O transmittance in Fig. 2 is reduced rather that what is seen in Fig. 1. The aminopropyl and SiO_2 vibration at 2,808 and 991–1,221 cm^{-1} clearly approved the aminopropyltriethoxysilanation process [18–21].

3.1.2. X-ray diffraction pattern

Fig. 3 shows the X-ray diffraction pattern on iron oxide nanocrystals. The reflection peaks at 2θ = 30.0, 35.6, 43.8, 54.2, 57.2, and 62.5 were indexed to (2 2 0) (3 1 1) (4 0 0) (4 2 2) (5 1 1), and (4 4 0) plans are in agreement with the database of magnetite. It is indicated that the iron oxide nanocrystals had a crystalline cubic spinel structure. The mean crystalline size of magnetic nanocrystals was determined using Debye–Scherrer method. According to Debye–Scherrer

method, the full width-half maximum (FWHM) of a reflection peak counts the mean crystalline size of a particle as [21]:

$$D = \frac{k\lambda}{\beta \cos \theta} \tag{2}$$

where D is the crystalline mean size, λ is the radiation wavelength, and β is FWHM in radians at 2θ. The mean crystalline size of the synthesized nanocrystals was calculated as 11.3 nm.

3.1.3. Scanning electron microscope

The morphology of the nanocrystals was examined by direct observation via scanning electron microscopy (SEM). The micrograph of nanocrystals is given in Fig. 4. It is clear from Fig. 4 that the synthesized particles are non-uniform with amorph surfaces. The mean diameter of nanocrystals, measured by SEM is larger than the mean size of nanocrystals obtained by X-ray
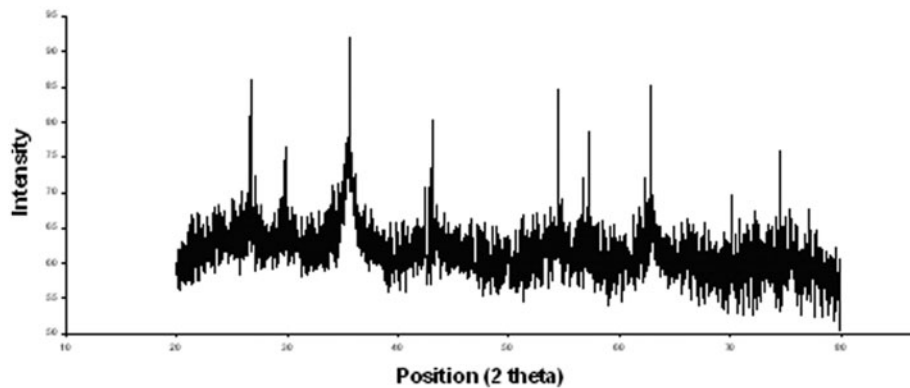
Fig. 3. XRD diffraction pattern of superparamagnetic iron oxide nanocrystal.

diffraction. It may be due to the conglommerate state of nanocrystals. In fact, strong magnetic and electric forces in the superparamagnetic nanocrystals are not balanced in the bare nanocrystals which caused such agglomerates. However, coating nanocrystals with SiO_2 improved their morphology.

3.1.4. Brunauer-Emmet-Teller (BET) and potential of zero charge

Surface areas of superparamagnetic nanocrystal and superparamagnetic nanocrystal/SiO_2–NH_2 were measured according to Brunauer-Emmet-Teller (BET) procedure [22]. The results show that surface areas of superparamagnetic nanocrystal and superparamagnetic nanocrystal/SiO_2–NH_2 are 112.3 and 208.0 m^2/g, respectively.

The zero charge pH (pH_{zcp}) is defined as the zero pH in the net surface. The pH_{zcp} of superparamagnetic nanocrystal and superparamagnetic nanocrystal/SiO_2–NH_2 were determined experimentally. The pH_{zcp} was measured in pH range of 1–12. pH values were adjusted with aqueous solutions HCl and NaOH (0.1 M). 0.02 g of the nanocrystals was added to each solution (10 mL). The supernatant was decanted and its pH was measured (pH_{Final}). The pH_{zcp} value was determined as the point at which the curve of pH_{Final} vs. $pH_{Initial}$ intersects the line $pH_{Initial} = pH_{Final}$. The pH_{zcp} of superparamagnetic Iron oxide nanocrystal/ SiO_2 was about 2.8, which is in agreement with the literature [23,24].

3.2. Adsorption experiment

After synthesis and characterization of iron oxide/ SiO_2–NH_2 nanocrystals, the viability of BPA adsorption by nanocrystals was demonstrated. Adsorption equilibrium depends on the adsorbent/adsorbate characteristics, time, temperature, and the amount of target species.
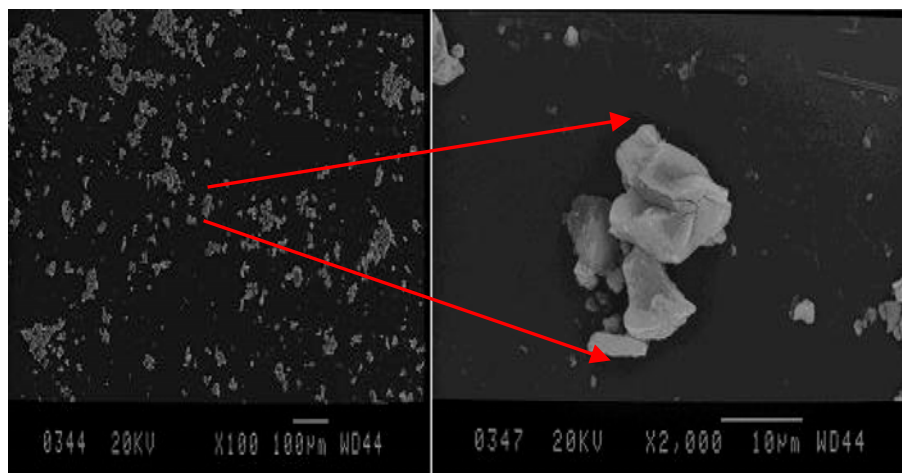

Fig. 4. SEM micrograph of superparamagnetic Iron oxide nanocrystal.

3.3. Optimization of adsorption parameters

The optimization of experimental parameters was carried out for BPA adsorption. The pH of the solution affects the surface charge of the nanocrystal, degree of ionization of the materials, and dissociation of functional groups on the adsorbent. As well, it affects both the structure of the BPA molecule and nanocrystal surface [25]. The sorption capacity of nanocrystal as a function of pH is plotted in Fig. 5. The sorption capacity increased from 5 to 35 when pH was increased from 2 to 6. This was because the BPA molecule adsorbed easily even in inert media. As the initial solution pH decreased, the number of positively charged active sites increased due to the protonation of the amine groups (–NH$_2$) in the nanocrystal chain. Consequently, the electrostatic interaction between the positively charged adsorbent and the BPA A increased, which resulted in increased adsorption. Therefore, higher removal percentages were observed at inert pH values. The effect of adsorbent dosage (varied from 0.15 to 0.25 g) on the sorption capacity of 4 mg/L BPA solution is shown in Fig. 6. The sorption capacity of BPA from the solution increased from 10 to 40 as the adsorbent dosage increased from 0.15 to 0.25 g. This result is expected because of the increased adsorbent surface area and availability of more adsorption sites caused by increasing adsorbent dosage [26,27].

To study the effect of shaking time on the sorption capacity, 4 mg/L of BPA was taken in conical flasks and treated with 0.2 mg adsorbent (nanocrystal) at several times (5–50 min). The variation in sorption capacity of nanocrystal with the time was shown in Fig. 7. The sorption capacity increased from 10 to 42 when time was increased from 5 to 50 min, this was due to saturation of active sites which do not allow further adsorption to take place [28].
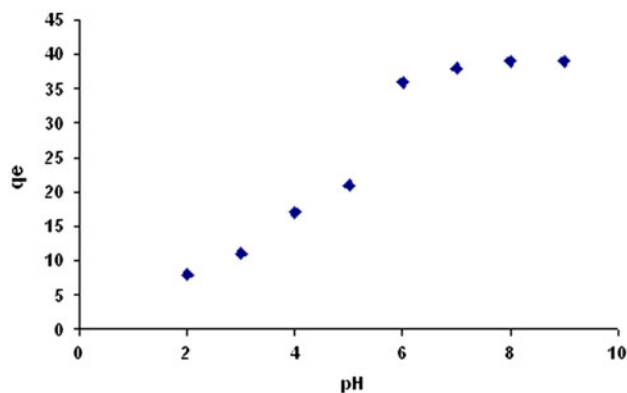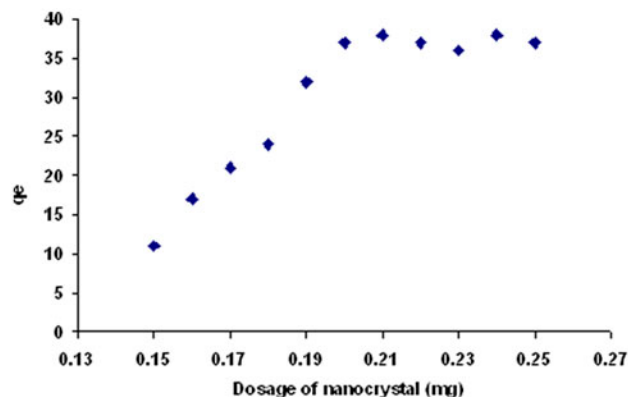

Fig. 6. Effect of superparamagnetic Iron oxide nanocrystal/ SiO$_2$–NH$_2$ dosage on the adsorption of BPA.
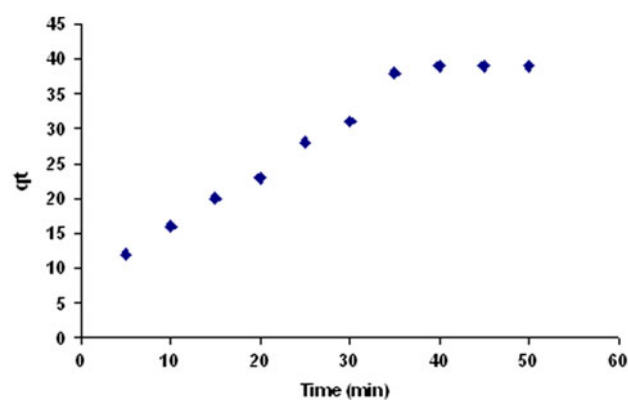

Fig. 7. Effect of shaking time on the adsorption of BPA onto superparamagnetic Iron oxide nanocrystal/SiO$_2$–NH$_2$.

3.4. Adsorption kinetics

Adsorption kinetic study is useful to predict the adsorption rate in order to gain the important information for sketching and modeling of the sorption process [29]. In order to obtain the adsorption behavior of iron oxide/SiO$_2$–NH$_2$ nanocrystals, the kinetics of BPA adsorption was studied. The kinetic rate equation is shown by:

$$\frac{dq_t}{dt} = k^2 \cdot (q_e - q_t)^2 \tag{3}$$

Integration with the boundary conditions $q_t = 0$ at $t = 0$ and $q_e = q_t$ at $t = t$, Eq. (3) reads:

$$\frac{t}{q_t} = \frac{t}{q_e} + \frac{1}{k_2} \frac{1}{q_e^2} \tag{4}$$

Fig. 5. Effect of pH on the adsorption of BPA onto superparamagnetic Iron oxide nanocrystal/SiO$_2$–NH$_2$.

Table 1
Kinetics model parameters for BPA sorption on superparamagnetic Iron oxide nanocrystal/SiO_2–NH_2

Pseudo-second-order model		
K_2	$q_{e,Cal}$	R^2
0.024	186.1	0.99

where q_e and q_e are amounts (mg g^{-1}) BPA at equilibrium and time t, respectively. K_2 is the pseudo-second-order rate constant. Various sorption kinetic models including first-order and pseudo-second-order kinetics were applied to the adsorption data. The values of the kinetic parameters for the sorption are given in Table 1. As shown in Table 1, the correlation coefficient of the psudo-second-order model is 0.99 which is higher than the first-order kinetic model correlation coefficient (0.84). So the adsorption of BPA onto iron oxide/SiO_2–NH_2 nanocrystals can be well described by the psudo-second-order kinetic model. This suggests that the adsorption may not by limited by the rate-limiting step.

3.5. Adsorption isotherms

The adsorption isotherms represent the adsorbate molecules distribution between the liquid phase and solid phase at the equilibrium state. Main adsorption isotherms including Langmuir and Freundlich were widely applied to obtain the sorption isotherm model of adsorption systems. The Langmuir adsorption isotherm is based on the assumption that the monolayer adsorption occurs on the homogeneous surface of the adsorbent without interaction between the absorbed molecules [29]. The Langmuir isotherm can be shown by Eq. (5):

$$\frac{C_e}{q_e} = \left(\frac{C_e}{q_m}\right) + \left(\frac{1}{K_L q_m}\right) \tag{5}$$

where K_L is the Langmuir adsorption equilibrium constant (L mg^{-1})and C_e is the equilibrium BPA concentration (mg L^{-1}), q_e is the amount of BPA adsorbed per unit of adsorbent (mg g^{-1}) at equilibrium concentration C_e and q_m is the maximum Adsorption capacity (mg g^{-1}), which depends on the number of adsorption sites.

The Freundlich isotherm model is [30]:

$$q_e = \frac{q_m b C_e}{1 + b C_e} \tag{6}$$

where q_e (mmol/L) and C_e (mmol/L) are the adsorbed concentration and total concentration at the equilibrium time. q_m (mmol/g) is the adsorption capacity, and b (L/mmol) is the affinity coefficient. To explore the adsorption mechanism much deeply, we studied the adsorption isotherms of BPA molecule onto iron oxide/SiO_2–NH_2 nanocrystals. It was found that al low initial BPA concentrations, nanocrystals exhibit high adsorption percentage, however, in high BPA concentrations, the adsorption capacity steadily raise. The adsorption isotherms of BPA onto the iron oxide/SiO_2–NH_2 nanocrystals as a function of BPA concentration and at pH 6–35 min adsorption time are shown in Figs. 8a and 8b and related Langmuir and
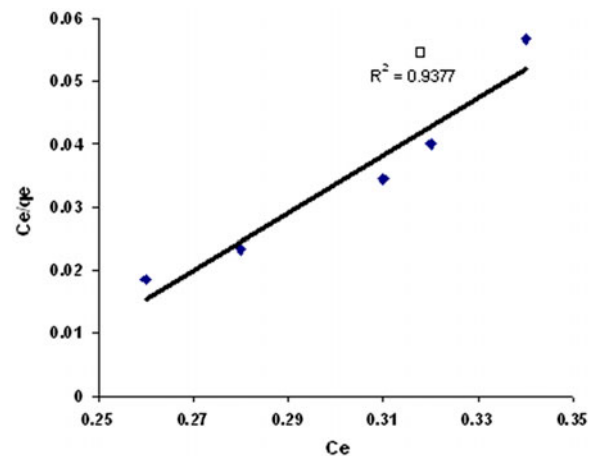
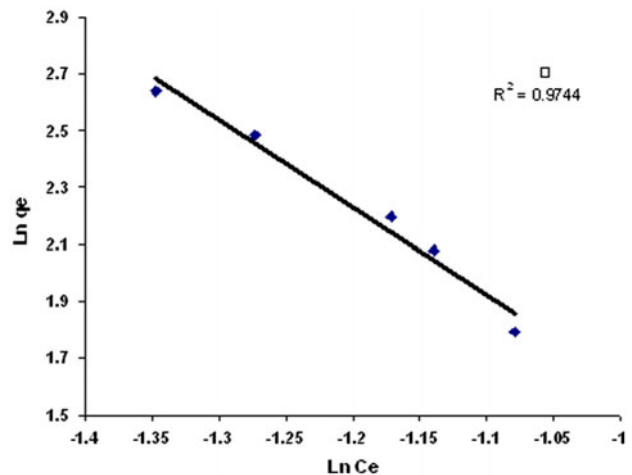Fig. 8a. Adsorption isotherm (Langmuir) of BPA on superparamagnetic Iron oxide nanocrystal/SiO_2–NH_2.

Fig. 8b. Adsorption isotherm (Freundlich) of BPA on superparamagnetic Iron oxide nanocrystal/SiO_2–NH_2.

Table 2
Isotherm model parameters for BPA sorption on superparamagnetic Iron oxide nanocrystal/SiO_2–NH_2

Langmuir model			Freundlich model		
q_{max}	K_L	R^2	K_f	n	R^2
198.2	−4.428	0.9377	0.2326	−0.325	0.9744

Freundlich constants are presented in Table 2. As shown in Table 2, the higher correlation coefficient of Freundlich model indicates that the Freundlich model fit the adsorption data better than the Langmuir model.

4. Conclusion

Removal of BPA as in environmental water samples is very important today. One of the methods of BPA adsorption is using iron oxide nanocrystals. In this paper, superparamagnetic iron oxide/SiO_2–NH_2 was synthesized via facile, fast, and low-cost process and further was developed to be highly efficient adsorbent for BPA in aqueous solution. SiO_2 reduces the serious stacking of superparamagnetic iron oxide and prevents the agglomeration of nanocrystals, and also produces a high tunable surface area, which enables high binding capability and excellent adsorption properties for BPA. This adsorbent is stable, low-cost, and environmentally friendly and shows potential application in the removal of BPA.

References

[1] C.C. Willhite, G.L. Ball, C.J. McLellan, Derivation of a bisphenol A oral reference dose (RfD) and drinking-water equivalent concentration, J. Toxicol. Environ. Health Part B 11 (2008) 69–146.

[2] A.M. Calafat, X. Ye, L.Y. Wong, J.A. Reidy, L.L. Needham, Exposure of the U.S. population to bisphenol A and 4-tertiary-octylphenol: 2003–2004, Environ. Health Perspect. 116 (2008) 39–44.

[3] L.N. Vandenberg, T. Colborn, T.B. Hayes, J.J. Heindel, D.R. Jacobs Jr, D.H. Lee, T. Shioda, A.M. Soto, F.S. vom Saal, W.V. Welshons, Hormones and endocrine-disrupting chemicals: Low-dose effects and nonmonotonic dose responses, Endocr. Rev. 33 (2012) 378–455.

[4] U. Chhaya, A. Gupte, Possible role of laccase from fusarium incarnatum UC-14 in bioremediation of bisphenol A using reverse micelles system, J. Hazard. Mater. 254–255 (2013) 149–156.

[5] K. Modaressi, K.E. Taylor, J.K. Bewtra, N. Biswas, Laccase-catalyzed removal of bisphenol-A from water: Protective effect of PEG on enzyme activity, Water Res. 39 (2005) 4309–4316.

[6] T.A. Ternes, M. Stumpf, J. Mueller, K. Haberer, R.D. Wilken, M. Servos, Behavior and occurrence of estrogens in municipal sewage treatment plants—I. Investigations in Germany, Canada and Brazil, Sci. Total Environ. 225 (1999) 81–90.

[7] W.-T. Tsai, C.-W. Lai, T.-Y. Su, Adsorption of bisphenol-A from aqueous solution onto minerals and carbon adsorbents, J. Hazard. Mater. 134 (2006) 169–175.

[8] B. Pan, D. Lin, H. Mashayekhi, B. Xing, Adsorption and hysteresis of bisphenol A and 17α-ethinyl estradiol on carbon nanomaterials, Environ. Sci. Technol. 42 (2008) 5480–5485.

[9] L. Joseph, Q. Zaib, I.A. Khan, N.D. Berge, Y.-G. Park, N.B. Saleh, Y. Yoon, Removal of bisphenol A and 17α-ethinyl estradiol from landfill leachate using single-walled carbon nanotubes, Water Res. 45 (2011) 4056–4068.

[10] J. Li, B. Zhou, Y. Liu, Q. Yang, W. Cai, Influence of the coexisting contaminants on bisphenol A sorption and desorption in soil, J. Hazard. Mater. 151 (2008) 389–393.

[11] W. Han, L. Luo, S. Zhang, Adsorption of bisphenol A on lignin: Effects of solution chemistry, Int. J. Environ. Sci. Technol. 9 (2012) 543–548.

[12] R. Gong, J. Liang, F. Huang, Removal of bisphenol A from aqueous solution by hydrophobic sorption of hemimicelles, Int. J. Environ. Sci. Technol. 6 (2009) 539–544.

[13] Q. Sui, J. Huang, Y. Liu, X. Chang, G. Ji, S. Deng, T. Xie, G. Yu, Rapid removal of bisphenol A on highly ordered mesoporous carbon, J. Environ. Sci. 23 (2011) 177–182.

[14] F.-X. Qin, S.-Y. Jia, Y. Liu, H.-Y. Li, S.-H. Wu, Adsorptive removal of bisphenol A from aqueous solution using metal-organic frameworks, Desalin. Water Treat. 54 (2015) 93–102.

[15] W. Yang, A.T. Kan, W. Chen, M.B. Tomson, pH-dependent effect of zinc on arsenic adsorption to magnetite nanoparticles, Water Res. 44 (2010) 5693–5701.

[16] C.T. Yavuz, J.T. Mayo, C. Suchecki, Pollution magnet: Nano-magnetite for arsenic removal from drinking water, Environ. Geochem. Health 32 (2010) 327–334.

[17] Y. Jeong, M. Fan, S. Singh, C.L. Chuang, B. Saha, J. Hans van Leeuwen, Evaluation of iron oxide and aluminum oxide as potential arsenic(V) adsorbents, Chem. Eng. Process. 46 (2007) 1030–1039.

[18] J. Wang, S. Zheng, Y. Shao, J. Liu, Z. Xu, D. Zhu, Amino-functionalized Fe_3O_4@SiO_2 core–shell magnetic nanomaterial as a novel adsorbent for aqueous heavy metals removal, J. Colloid Interface Sci. 349 (2010) 293–299.

[19] Y.F. Huang, Y.F. Wang, X.P. Yan, Amine-functionalized magnetic nanoparticles for rapid capture and removal of bacterial pathogens, Environ. Sci. Technol. 44 (2010) 7908–7912.

[20] M. Yamaura, R.L. Camilo, L.C. Sampaio, M.A. Macêdo, M. Nakamura, H.E. Toma, Preparation and characterization of (3-aminopropyl)triethoxysilane-coated magnetite nanoparticles, J. Magn. Magn. Mater. 279 (2004) 210–217.

[21] T.Z. Yang, C.M. Shen, H.J. Gao, Highly ordered self-assembly with large area of Fe_3O_4 nanoparticles and the magnetic properties, J. Phys. Chem. B 109 (2005) 23233–23236.

[22] S. Brunauer, P.H. Emmett, E. Teller, Adsorption of gases in multimolecular layers, J. Am. Chem. Soc. 60 (1938) 309–319.

[23] S. Ahmaruzzaman, L. Gayatri, Batch adsorption of 4-nitrophenol by acid activated jute stick char: Equilibrium, kinetic and thermodynamic studies, Chem. Eng. J. 158 (2009) 173–180.

[24] A. Penkova, J.M. Martínez Blanes, S.A. Cruz, M.A. Centeno, K. Hadjiivanov, J.A. Odriozola, Gold nanoparticles on silica monospheres modified by amino groups, Microporous Mesoporous Mater. 117 (2009) 530–534.

[25] Z. Aksu, S. Ertuğrul, G. Dönmez, Methylene blue biosorption by rhizopus arrhizus: Effect of SDS (sodium dodecylsulfate) surfactant on biosorption properties, Chem. Eng. J. 158 (2010) 474–481.

[26] A. Farmany, S.S. Mortazavi, High adsorption capacity of multi-walled carbon nanotube as efficient adsorbent for removal of Al(III) from wastewater, Part. Sci. Technol. 33 (2015) 423–428.

[27] H. Chen, J. Zhao, A. Zhong, Y. Jin, Removal capacity and adsorption mechanism of heat-treated palygorskite clay for methylene blue, Chem. Eng. J. 174 (2011) 143–150.

[28] H. Faghihian, H. Nourmoradi, M. Shokouhi, Removal of copper (II) and nickel (II) from aqueous media using silica aerogel modified with amino propyl triethoxysilane as an adsorbent: equilibrium, kinetic, and isotherms study, Desalin. Water Treat. 52 (2014) 305–313.

[29] I. Langmuir, The constitution and fundamental properties of solids and liquids. Part I. Solids, J. Am. Chem. Soc. 38 (1916) 2221–2295.

[30] H. Freundlich, Colloid and Capillary Chemistry, Metheum, London, 1926, pp. 993.